Journal of Fluorescence (2020) 30:1345–1355
https://doi.org/10.1007/s10895-020-02613-z

ORIGINAL ARTICLE

Synthesis, Structure Study, First-Principles Investigations and Luminescence Properties of Europium and Terbium Complexes

Bakhat Ali[1,2] · Helio A. Stefani[1] · Muhammad Imran[3,4] · Ahmad Irfan[3,5] · Mohammed A. Assiri[3] · Maria Claudia F. C. Felinto[6] · Muhammad Khalid[2] · Abdullah G. Al-Sehemi[3]

Received: 20 June 2020 / Accepted: 24 August 2020 / Published online: 1 September 2020

Abstract

The synthesis of 1-benzyl-2-((2-Aminoethyl) amino)-5-oxopyrrolidine-3,4-diyl diacetate (boad), an oxopyrrolidine type ligand; designed to coordinate lanthanides (Eu^{3+} and Tb^{3+}) to get luminescent material. The target complexes showed good photoluminescence properties, which indicate that this type of compound can be used as sensitizers having luminescence for the green (Tb^{3+}) and red (Eu^{3+}) emission. The obtained results revealed that sensitizer efficiency can be improved by adding ligands like acac ($Eu(acac)_3$, which has also enhanced the luminescence quantum output and period for Eu^{3+} ions. The ground state geometries were developed by using density functional theory at B3LYP/6-31G** level. The charge transfer analysis and electronic properties were performed. The Europium and Terbium complexes formation with boad ligand was explored based on molecular electrostatic potential, MDC-q charges, and *frontier molecular orbitals* (*FMOs*) analysis.

Keywords Tartaric acid · Oxopyrrolidine · Europium · Terbium · Lanthanide complexes · Photoluminescence: Density functional theory

Introduction

The fluorescence-based sensors, solar thermophotovoltaic, and light-beam diodes (single-photon sources) are based on emission, which is not an intrinsic worth of luminescent material. Emission originates as a result of the interface between its electromagnetic environment and the material. The emission features changes with the alteration with modification of the environment have possible utilization with integrated photonics, sensing, and solar energy transformation [1]. Due to their light emission properties, lanthanide ion complexes have applications in areas ranging from fluoroimmunoassays to materials science [2].

The ligands play a key role in absorbing energy in demand to acquire strongly luminescent complexes. The lanthanide ions exhibit ample dimension with photonic utilization, like luminescent probes for analyses, amplifiers for optical transportations, tunable lasers, a segment of the emitting components within organic light-emitting diodes (multilayer), and efficient light transformation molecular equipment. [3–5]. When the rare earth ions are coordinated with ligands containing chromophores, the weak absorbance from the rare earth ion can be overcome to exhibit higher luminescence intensity. The ligand lowest energy level, i.e., triplet state (T_1) grants energy transfer within rare-earth ions to their excited state [6]. The Tb^{3+} and Eu^{3+} ions are having peculiar attention because of their lengthy luminescence lifetime and limited radiations line within the visible region. [7–9]. The organic and inorganic segment informally mixed with the hybrid component to establish a valuable class of materials accord

✉ Bakhat Ali
bakhatali@gmail.com

✉ Muhammad Imran
imranchemist@gmail.com

1 Departamento de Farmácia, Faculdade de Ciências Farmacêuticas, Universidade de São Paulo, São Paulo, SP, Brazil

2 Department of Chemistry, Khwaja Fareed University of Engineering and Information Technology, Rahim Yar Khan 64200, Pakistan

3 Department of Chemistry, Faculty of Science, King Khalid University, P.O. Box 9004, Abha 61413, Saudi Arabia

4 Department of Chemistry, Ghazi University Dera Ghazi Khan, Dera Ghazi Khan, Pakistan

5 Research Center for Advanced Materials Science (RCAMS), King Khalid University, P.O. Box 9004, Abha 61413, Saudi Arabia

6 Instituto de Pesquisas Energéticas e Nucleares, IPEN, São Paulo, SP 05508-900, Brazil

synergistic possessions that grant towards new performances having reinforced properties. These materials have applications in microelectronics, optics, batteries, photovoltaics, biology, and medicine [10, 11].

Our group has been working on oxopyrrolidine compounds [12–16]. We synthesized the 1-benzyl-2-((2-Aminoethyl) amino)-5-oxopyrrolidine-3,4-diyl diacetate (baod) compound and reacted with Eu^{3+} and Tb^{3+} ions to develop complexes that present emission of light. In the preliminary study, the ligand baod has gained very interesting properties, which has got interest in further luminescence study. With the aim to synthesize and characterize functional luminescent materials, we explored the electronic and optical properties of the 1-benzyl-2-((2-Aminoethyl) amino)-5-oxopyrrolidine-3,4-diyl diacetate ligand (baod) (by experimental and advanced computational approaches. Moreover, two new complexes of Eu^{3+} and one of Tb^{3+} were synthesized and characterized to study their photoluminescence and emission quantum efficiency of the emission process were measured.

Material and Methods

All commercial-grade starting substances used without further purification. ^{1}H-NMR (300 MHz), ^{13}C-NMR (75 MHz) spectra were reported with Bruker DPX 300, using $CDCl_3$ as a solvent. Infrared bands were recorded using an FTIR Spectrometer (Agilent Cary 630). Steady-state emission and excitation spectra determined at room temperature (~25 C), whereas 77 K temperatures for liquid nitrogen were reported. The Xenon lamp (450 W) as the excitation source and 22.51 (front face) angle using Fluorolog 3 spectrofluorimeter with 0.22 m monochromator double grating (SPEX 1680) were used. The spectral readings were documented with detector mode correction. This equipment was controlled by software FluorEssence 3.0. The curves for luminescence decay with emitting points were recorded using a SPEX 1934D phosphorimeter coupled to the spectrofluorometer. The $_{L}$-tartaric acid, acetyl chloride, benzylamine, sodium borohydrate, acetic anhydride, boron trifluoride etherate, europium oxide (Eu_2O_3), acetylacetone (acac), and terbium oxide (Tb_4O_7) were purchased from Sigma-Aldrich. The hydrated lanthanide (III) chloride hexahydrated($LnCl_3{\cdot}6H_2O$) was groomed using their respective oxide by reacting with HCl solution (concentrated) with complete disintegration of solid material having pH close to 6.0.

Procedure for Synthesis of Ligand [1-Benzyl-2-((2-Aminoethyl) Amino)- 5-Oxopyrrolidine-3,4-Diyl Diacetate] (Bao)

To a 25 mL 2-neck round bottom flask of 1-benzyl-5-oxopyrrolidine-triyl triacetate (**d**, 1 mmol) [12] was combined with 5 mL of dry DMSO under N_2 at room temperature. BF_3.etherate (1.2 eq) was mixed drop wise and resulting concoction was agitated at same temperature for 30 min with drop wise addition of 1,2 ethane diamine (3 mmol) and left for 2 h. The reaction completion was confirmed after the TLC and GC-MS analysis. After its completion 1 M HCl (10 mL) was added for quenching, extracted with solvent chloroform (3 × 26 mL), dried over $MgSO_4$ and concentrated under *vacuo* to get corresponding product (baod). Synthetic scheme is shown in (Scheme 1). FTIR (cm^{-1}): ν(N-H) 3197; ν(C=O) 1678; ν(C-N) 1499, ν(C=C) 1454, 1436, ν(ph) 1078; ^{1}HNMR (300 MHz, chloroform-d): 1.25 (t, J = 6.00, 12.00 Hz, 2H + NH), 2.02 (t, J = 3.00, 6.00 Hz, 2H), 2.13 (s, 6H), 2.63 (NH), 4.09 (t, J = 6.01, 15.00 Hz, 1H), 4.41 (s, 2H), 4.62 (1H, dd, J = 6.01, 15.01 Hz), 4.90 (1H, d, J = 15.01 Hz), 7.24–7.30 (m, 5H); ^{13}CNMR (75 MHz, chloroform-d): 21.09 (2C), 42.36, 44.85, 49.22, 65.20, 75.09, 79.46, 126.23, 127.87 (2C), 128.00, 128.70 (2C), 136.47, 173.20 (3C). The photoluminescence spectra resulted in maximum emission spectra at 510 nm.

General Procedure for Synthesis of Complexes (1, 2, 3)

The complexes ($[Eu(baod)_2(H_2O)_2]$ **1,** [Eubaod $(acac)_2H_2O]$ **2** and $[Tb(baod)_2(H_2O)_2]$ **3**) were prepared according to reference [8]. The ligand (1 mmol) was dissolved within ethanol (20 mL), potassium tert-butoxide (4 mmol) was mixed, followed by 30 min stirring. The $EuCl_3.6H_2O$ or $TbCl_3.6H_2O$ (0.5 mmol) was dissolved with the dropwise addition of EtOH, and left for 24 h magnetic stirring. The solvent was evaporated under vacuum to get residual molecules. Then washed with $CHCl_3$ and evaporated under high vacuum to get the respective complexes (Scheme 2).

$[Eu(baod)_2(H_2O)_2]$ (1): FTIR (in cm^{-1}): (N-H, H_2O) 3201, (C=O) 1674, (C-N) 1499, (C=C, CH_3) 1454, 1436, (ph) 1078, 702

$[Eu(baod)(acac)_2.H_2O]$ (2): FTIR (in cm^{-1}): (N-H, H_2O) 2921, (C=O) 1693, (C-N) 1547, (C=C, CH_3) 1413, 1346, (ph) 1231, 1022, 948, 702.

$[Tb(baod)_2(H_2O)_2]$ (3): FTIR (in cm^{-1}): (N-H, H_2O) 3033, 2940, (C=O) 1707, (C-N) 1454, (C=C, CH_3) 1436, 1372, (ph) 1223, 1078, 1033, 952, 706.

Computational Details

The first-principles approaches are fascinating tools to probe different properties of concern [17]. The forecasting of electronic properties systematically calculated by

Scheme 1 Synthesis of starting material 1-benzyl-2-((2-aminoethyl)amino)- 5-oxopyrrolidine-3,4-diyl diacetate (ligand)

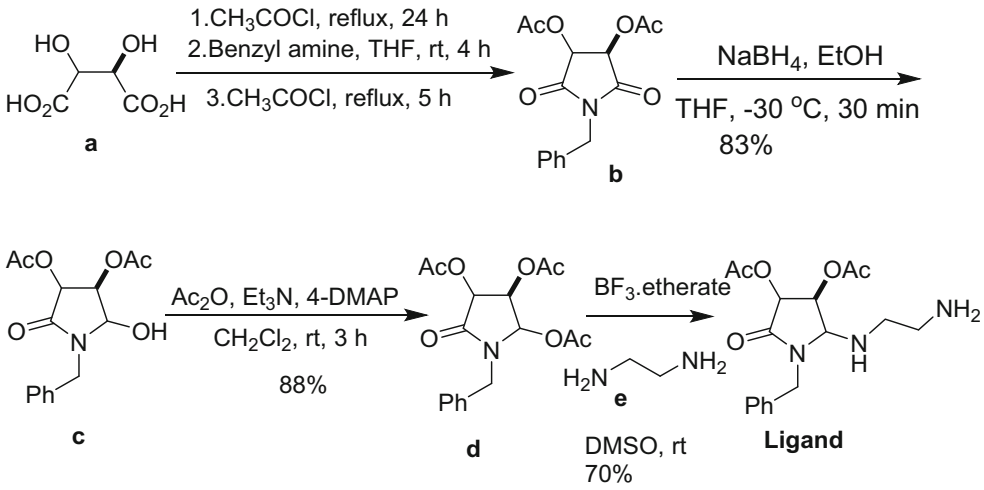

density functional theory (DFT) and meritoriously simulated the experimental data [18]. For the measurement of ground state (S_0) geometries and electronic properties, the DFT is a suitable approach. The DFT was found a compelling and decent path for the geometries optimizations (S_0) of various molecules [19]. The B3LYP is rational for the S_0 geometries in different molecules and their complexes [20]. Already, it was achieved that subsequently, geometries optimizing of the molecules using the B3LYP functional approach with an estimate of basis groups have no extraordinary effect on the geometrical specifications [21]. In the current examination, the optimizations were implemented with functional B3LYP and triple zeta with (TZ2P) 2 polarization function basis group [22]. ADF was used for the computational purposes.

Result and Discussion

Characterization

The organic linker ligands coordinate with the metal ions have attracted noteworthy attention in the fields of supramolecular chemistry, materials chemistry, polymer science, and inorganic chemistry [23]. Herein, we synthesized organic linker ligand (Scheme 1), which coordinates with lanthanide ions (Scheme 2), which gives luminescent material as novel phosphors. The organic linker synthesis was carried out using six steps. The main synthetic protocol is the synthesis of oxopyrrolidine and addition of ethylene-di-amine to acylium ion, generated by Lewis acid [7]. The synthetic ligand was confirmed by ^{1}H-, ^{13}C-NMR, and FTIR techniques.

Scheme 2 Structure of amino-oxopyrolidine luminescent materials: $[Eu(boad)_2(H_2O)_2]$ (**1**), $[Eu(boad)(acac)_2.H_2O]$ (**2**) and $[Tb(boad)_2(H_2O)_2]$ (**3**).

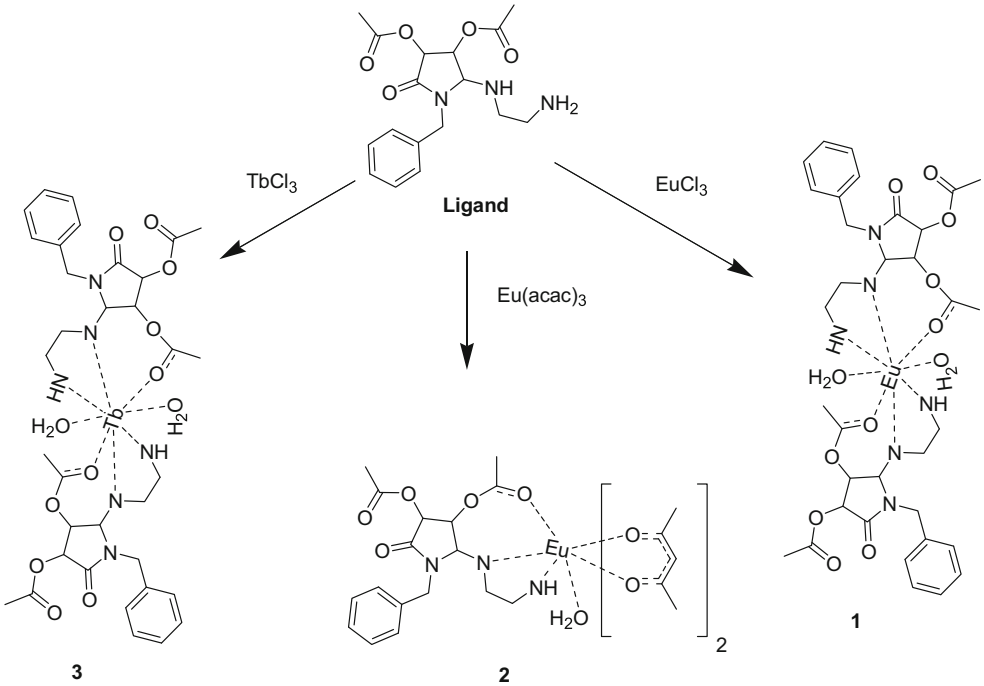

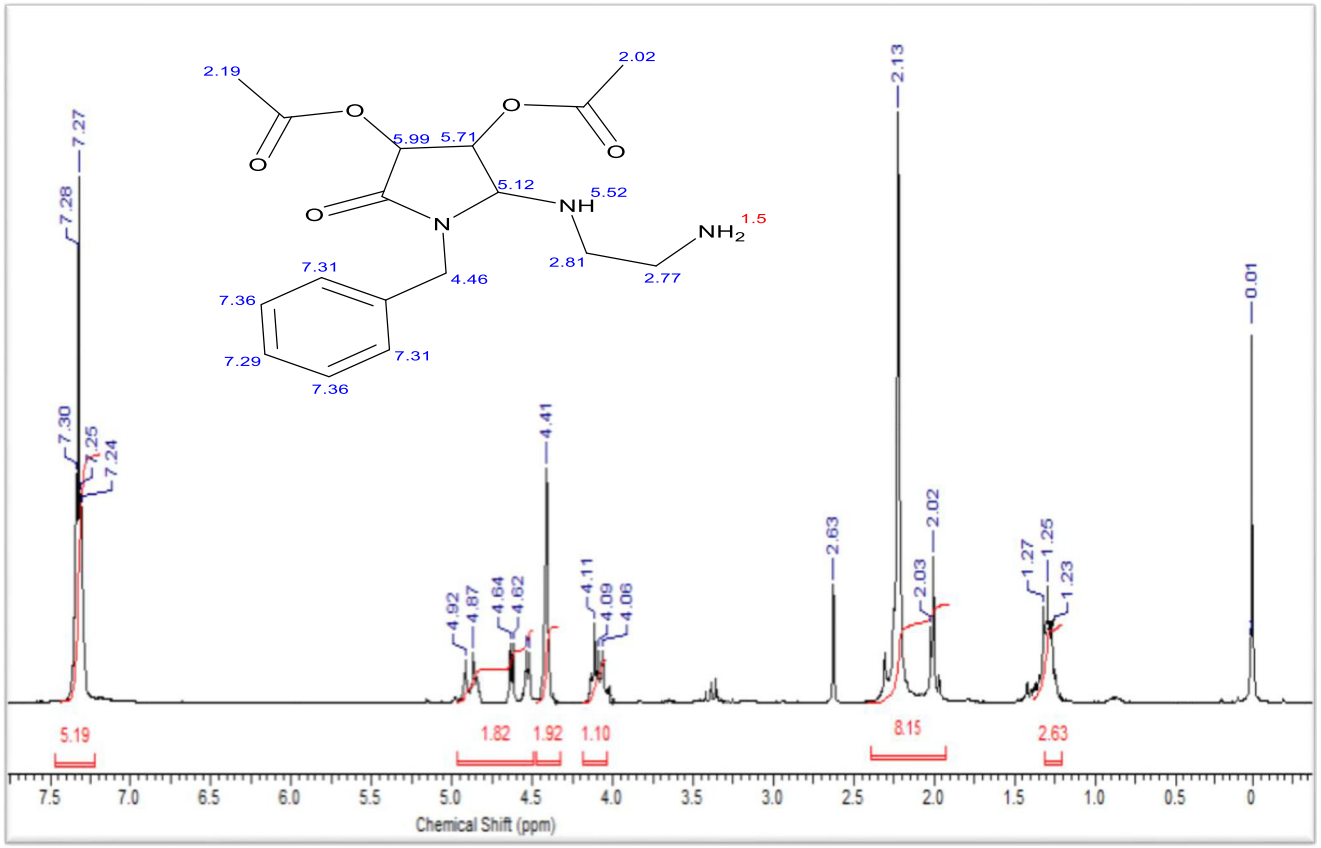

Fig. 1 [1]HNMR (300 MHz, chloroform-d) of 1-benzyl-2-((2-Aminoethyl) amino)- 5-oxopyrrolidine-3,4-diyl diacetate (baod)

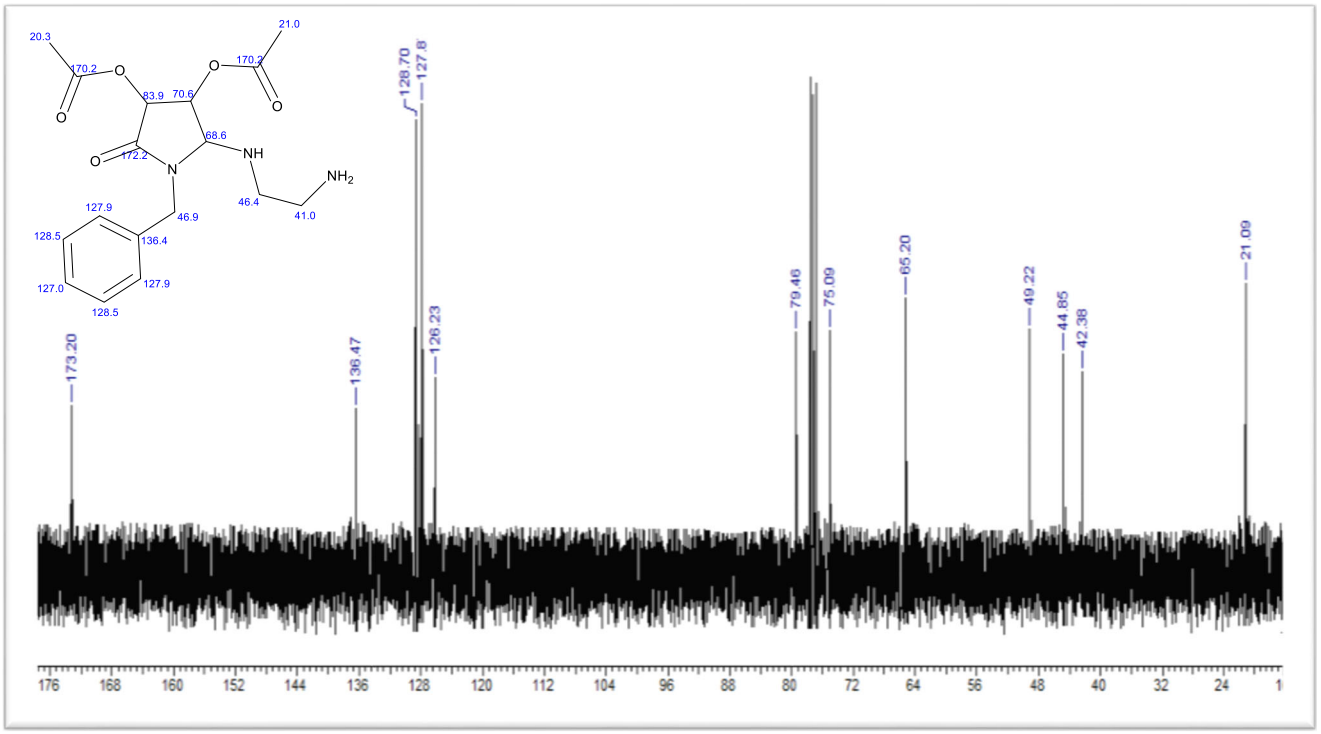

Fig. 2 [13]CNMR (75 MHz, chloroform-d) of 1-benzyl-2-((2-Aminoethyl) amino)- 5-oxopyrrolidine-3,4-diyl diacetate (baod)

NMR Spectra of Ligand

The ^{1}HNMR spectrum was recorded at room temperature (300 MHz, chloroform-d), which is showing a resonance peak at δ 1.25 and 2.02 for the 4H of methylene and amine protons (NH and NH_2) were resonating at δ 1.25 and 2.63 respectively. Additionally, broad singlet peak resonating at δ 2.13 relates to 6H of methyl (CH_3COO-). The methylene ($ArCH_2$-) protons

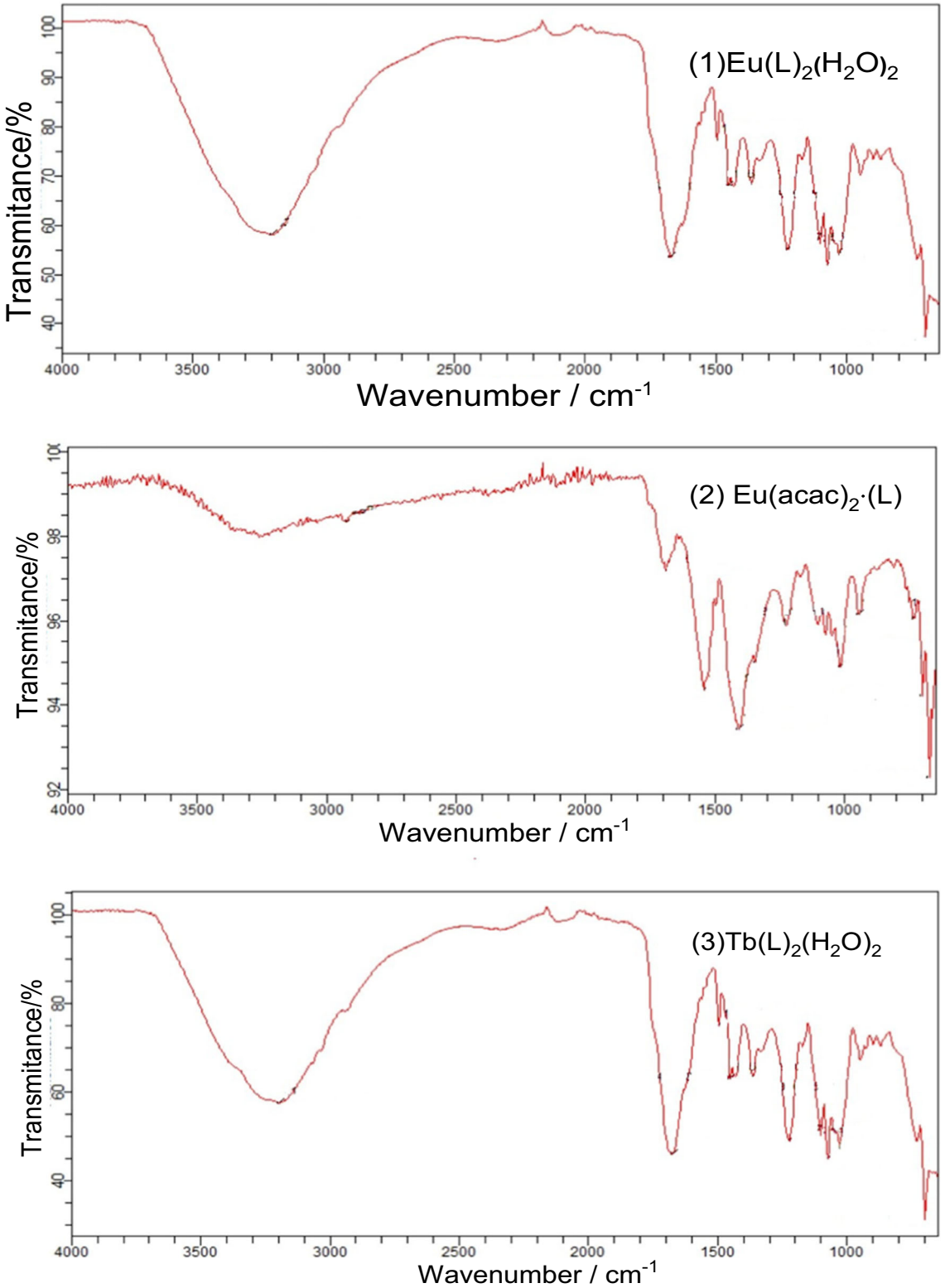

Fig. 3 FTIR absorption spectra of $[Eu(boad)_2(H_2O)_2]$ **1,** $[Eu(acac)_2(boad)H_2O]$ **2** and $[Tb(boad)_2(H_2O)_2]$ **3**

resonated at δ 4.41. The methine (CH) protons showing resonance peaks at δ 4.09, 4.62, and 4.90. The aromatic (Ar-) resonance peaks were observed at δ 7.24–7.30, as shown in Fig. 1. The ^{13}C NMR spectrum was recorded at room temperature (75 MHz, chloroform-d), which displays a resonance peak at δ 42.36 and 44.85 for methylene (-$NHCH_2CH_2$ NH_2). Similarly, other ^{13}C NMR resonance peaks are also evident with the reported oxopyrrolidine spectra [12], as shown in Fig. 2.

FTIR Spectra of Ligand and Complexes

The FTIR spectra of **baod** and complexes (**1**, **2** and **3**) show similar absorption peaks at around 1227 (N-H bending), and 1078 and 702 cm^{-1} corresponding to an aromatic moiety (C-H bending). Similarly, absorption bands at 1350–1550 cm^{-1} are assigned to stretching modes of C=C of the aromatic ring. The absorption bands observed at 1674–1707 cm^{-1}, which are due to asymmetric stretching and asymmetric stretching modes of carbonyl groups. A broad absorption band observed at around 3200 cm^{-1} is because of the ligand N-H stretching and also in the complex (1) as well, it indicates the presence of moisture contents. In complexes (**2** and **3**) weak absorption peaks around 2921–3033 cm^{-1} were observed due to stretching vibrations of C-H, as shown in Fig. 3.

Photoluminescence Investigations

The excitation spectra of $Eu(baod)_2(H_2O)_2]$ (**1**), $[Eu(acac)_2(boad)H_2O]$ (**2**) complexes were recorded in the spectral range from 250 to 550 nm (Fig. 4) monitored at the hypersensitive $^5D_0 \rightarrow {}^7F_2$ transition (~613 nm), at low temperature (77 K). The showing excitation narrow peaks at 394 nm, assigned to the $^7F_0 \rightarrow {}^5L_6$ transition of the Eu^{3+} ion. The broad excitation band centered at around 349 nm is assigned to the $S_0 \rightarrow S_1$ electronic transition of the acac ligand. Besides, it is observed narrow excitation peaks originated from the 4f-4f transitions of the Eu^{3+}-complexes such as: $^7F_0 \rightarrow {}^5D_1$ (535 nm), $^7F_0 \rightarrow {}^5D_2$ (465 nm), $^7F_0 \rightarrow {}^5D_3$ (415 nm), $^7F_0 \rightarrow {}^5L_6$ (394 nm), $^7F_0 \rightarrow {}^5L_7$ (375 nm) and $^7F_0 \rightarrow {}^5D_4$ (362 nm) [23, 24].

In addition, Fig. 4 shows the broad excitation band at 303 nm the attributed to the $S_0 \rightarrow S_1$ transition of the baod ligand as well as the narrow excitation peaks arising from the $^7F_6 \rightarrow {}^5D_4$ (486 nm), $^7F_6 \rightarrow {}^5L_{10}$ (368 nm), $^7F_6 \rightarrow {}^5G_5$ (358 nm) and $^7F_6 \rightarrow {}^5L_6$ (352 nm) transitions of the metal ion in the $[Tb(boad)_2(H_2O)_2]$ complex. Therefore, the highest excitation intensity of $S_0 \rightarrow S_1$ transition of the baod ligand compared with 4f-4f transitions of Tb^{3+}-complex indicates the highest intermolecular transfer energy efficiency from the ligand to the metal ion, as well as compared to the Eu^{3+} complexes.

The emission spectra of the Eu^{3+}-complexes recorded range from 400 to 750 nm (Fig. 5) under excitation of

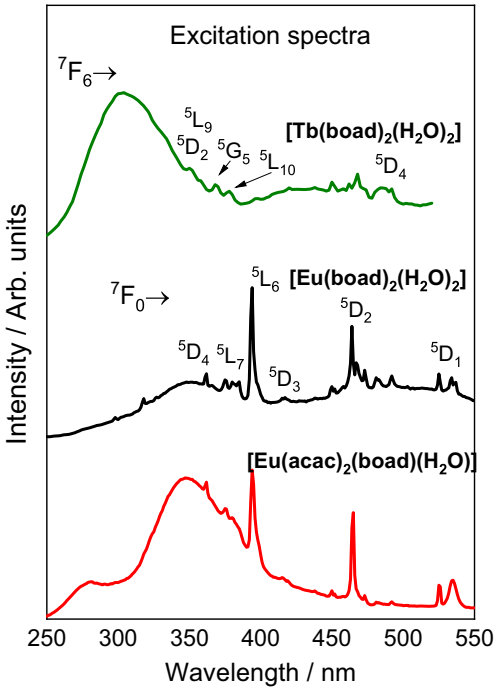

Fig. 4 Excitation spectra of the $[Eu(boad)_2(H_2O)_2]$ (**1**), $[Eu(boad)(acac)_2.H_2O]$ (**2**) and $[Tb(boad)_2(H_2O)_2]$ (**3**) complexes monitored at emission at ~613 and 550 nm respectively

$^7F_0 \rightarrow {}^5L_6$ (~394 nm), at 77 K present a high phosphorescence broadband intensity centered at 510 nm assigned to the triplet state (T_1) of the organic ligand. Besides, it is observed the narrow emission bands

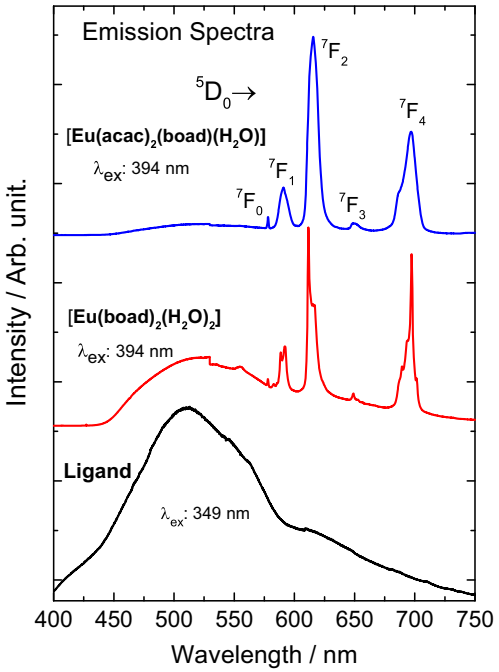

Fig. 5 Emission spectra of the ligand, $[Eu(boad)_2(H_2O)_2]$ (**1**), $[Eu(boad)(acac)_2.H_2O]$ (**2**) and $[Tb(boad)_2(H_2O)_2]$ (**3**) complexes under excitation at 394 and 349 nm

Table 1 Experimental intensity parameters (Ω_λ), emission quantum efficiency ($Q_{Eu^{3+}}^{Eu^{3+}}$) non-radiative (A_{nrad}), radiative (A_{rad}), and total emission (A_{tot}) rates at the room temperature for the $[Eu(baod)_2(H_2O)_2]$ and $[Eu(acac)_2(baod)(H_2O)_2]$ complexes have been calculated

Compounds	Ω_2 (10^{-20} cm^2)	Ω_4 (10^{-20} cm^2)	A_{rad} (s^{-1})	A_{nrad} (s^{-1})	A_{tot} (s^{-1})	$Q_{Eu^{3+}}^{Eu^{3+}}$ (%)
$[Eu(baod)_2(H_2O)_2]$ (**1**)	7.1	14.9	489	4198	4687	10
$[Eu(acac)_2(baod)(H_2O)_2]$ (**2**)	6.4	9.8	389	1482	1871	21
$[Eu(acac)_3(H_2O)_3]^*$	29	11	757	2609	3366	31

*[27]

attributed to the $^5D_0 \rightarrow {}^7F_0$ (578 nm), $^7F_1$ (591), $^7F_2$ (613), $^7F_3$ (650 nm), and $^7F_4$ (694 nm), transitions of the europium ion in the $[Eu(boad)_2(H_2O)_2]$ and [Eu(boad)(acac)$_2$H$_2$O] complexes. The presence of the $^5D_0 \rightarrow {}^7F_0$ transition at 578 nm for the Eu^{3+}-complexes indicates the symmetry sites C_n, C_{nv}, or C_s. As can be seen, Fig. 5 shows the broad emission band more prominent for the $[Eu(boad)_2(H_2O)_2]$ complex than for $[Eu(boad)(acac)_2(H_2O)]$, suggesting that the energy transfer from the triplet state (T_1) of the ligands to the excited $^5D_1$ and $^5D_0$ levels are more efficient for the compound that contain sensitizer acac ligand. [23–26]. It is noteworthy that the emission and excitation spectra of the prepared Ln^{3+}-complexes recorded at room (300 K) and low (77 K) temperatures show similar spectral profiles. However, the spectra obtained at liquid nitrogen temperature showed higher resolutions.

The $A_{0\rightarrow J}$ spontaneous emission coefficients for Eu^{3+}-complexes are calculated by using the $^5D_0 \rightarrow {}^7F_{0,1,2,3,4}$ transitions from the emission spectra (Fig. 5), using the $^5D_0 \rightarrow {}^7F_1$ transition as an internal reference given by eq. 1: [25].

$$A_{0\rightarrow J} = \left(\frac{S_{0\rightarrow J}}{S_{0\rightarrow 1}}\right) A_{0\rightarrow 1} \tag{1}$$

where $S_{0\rightarrow 1}$ and $S_{0\rightarrow J}$ correspond to the areas under the emission bands for the $^5D_0 \rightarrow {}^7F_1$ and $^5D_0 \rightarrow {}^7F_{J=2,4}$ transitions, respectively.

The Ω_2 experimental intensity parameter is very sensitive to the small angular changes in the local coordination geometry. On the other hand, the Ω_4 values are sensitive to the bond length and covalency. Therefore, The Ω_2 and Ω_4 intensity parameters can be calculated according to the expression (Eq. 2):

$$\Omega_\lambda = \frac{3\hbar c^3 A_{0\rightarrow\lambda}}{4e^2\omega^3\chi\langle {}^7F_\lambda \| U^{(\lambda)} \| {}^5D_0\rangle^2} \tag{2}$$

where $\chi = n(n^2+2)^2/9$ is the Lorentz correction term for the local field and $\langle {}^7F_\lambda \| U^{(\lambda)} \| {}^5D_0 \rangle^2$ is the square of the doubly reduced matrix element and the 0.0032 and 0.0023 values correspond for $\lambda = 2$ and 4, respectively. We have used the index of refraction $n = 1.5$ for the Eu^{3+}-complexes in the solid-state.

The lower values of Ω_2 parameters of the $[Eu(baod)_2(H_2O)_2]$ and $[Eu(acac)_2(baod)(H_2O)_2]$ complexes compared to that of the $[Eu(acac)_3(H_2O)_3]$ indicated a higher centrosymmetric site character around the europium ions (Table 1). On the other hand, the highest valor of the Ω_4 parameter of the $[Eu(baod)_2(H_2O)_2]$ suggests that this compound presents the highest polarization character compared to the other two europium complexes reported in Table 1.

The intrinsic quantum yield ($Q_{Eu^{3+}}^{Eu^{3+}}$) of $[Eu(boad)_2(H_2O)_2]$ and [Eu(boad)(acac)$_2$.H$_2$O] complexes depends on the radiative (A_{rad}), and non-radiative (A_{nrad}) rates due to multiphonon deactivation processes of the emitting level are given by expression (Eq. 3): [25].

$$Q_{Eu^{3+}}^{Eu^{3+}} = \frac{A_{rad}}{A_{rad} + A_{nrad}} \tag{3}$$

Where the A_{rad} rate values are calculated by the sum of the radiative contributions of the Eu^{3+} transitions ($A_{rad} = \sum_J A_{0\rightarrow J}$) and the A_{tot} values are obtained from the lifetimes (τ) of the $^5D_0$ emitting level by using the ratio $A_{tot} = 1/\tau = A_{rad} + A_{nrad}$.

The effectiveness of the emission process was also measured by the luminescence decay curves. The lifetime values for the Eu^{3+}-complex **1** is 0.213 ms, and for **2** is

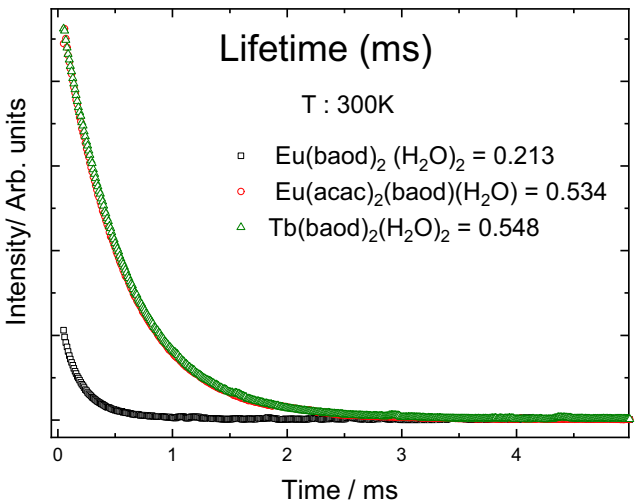

Fig. 6 Luminescence decay curves of the $[Eu(baod)_2(H_2O)_2]$ (**1**), [Eu.baod(acac)$_2$.H$_2$O] (**2**) and $[Tb(baod)_2(H_2O)_2]$ (**3**) complexes

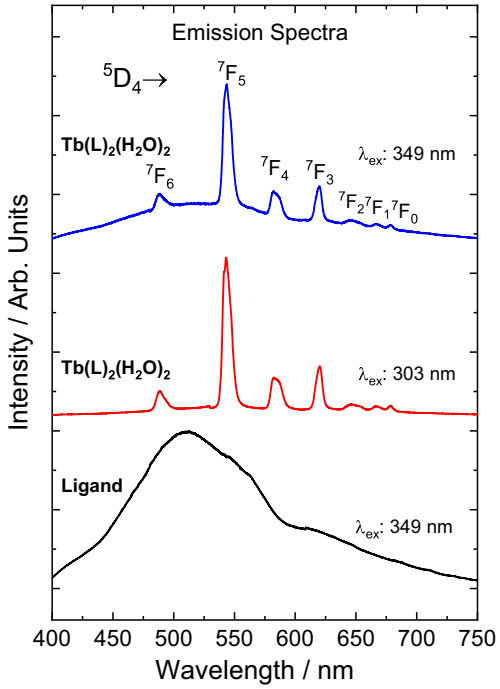

Fig. 7 Emission spectra of the ligand and $[Tb(L)_2(H_2O)_2]$ under excitation at 303 and 349 nm

0.534 ms, respectively. The higher decay lifetime is undoubtedly recognized to the further proficient interaction of the delocalized N and O atoms electronic pairs within ligand and metal ion. Similarly, lower decay lifetimes are due to the weaker interaction of ligand atoms and metal ions. In addition, the lifetime value for the Tb complex **3** is 0.548 ms, showing stronger interaction than europium complexes, as shown in Fig. 6.

The $Q_{Eu^{3+}}^{Eu^{3+}}$ values of all hydrated Eu^{3+}-complexes are not so high due to the increase in the non-radiative process rates (A_{nrad}), since the coupling between the emitting $^5D_0$ level of the Eu^{3+} ion and O-H oscillators of the water molecules is very strong. Besides, the boad organic ligand in $[Eu(baod)_2(H_2O)_2]$ complex also contributes to the non-radiative process, showing the highest of A_{nrad} value (4198 s^{-1}) [25].

Similarly, the emission spectra of the $[Tb(boad)_2(H_2O)_2]$ terbium complex and ligand were recorded at the spectral range from 400 to 750 nm at 77 K (Fig. 7). These spectra show the characteristic emission bands assigned to the $^5D_4 \rightarrow {}^7F_J$ (J = 6–0) transitions of the Tb^{3+} ions. The highest emission intensity band from terbium ion is attributed to the $^5D_4 \rightarrow {}^7F_5$ transition at around 550 nm, leading to the green emission color [28]. Moreover, the emission spectrum of Tb^{3+}-complex under excitation at 303 nm shows no emission

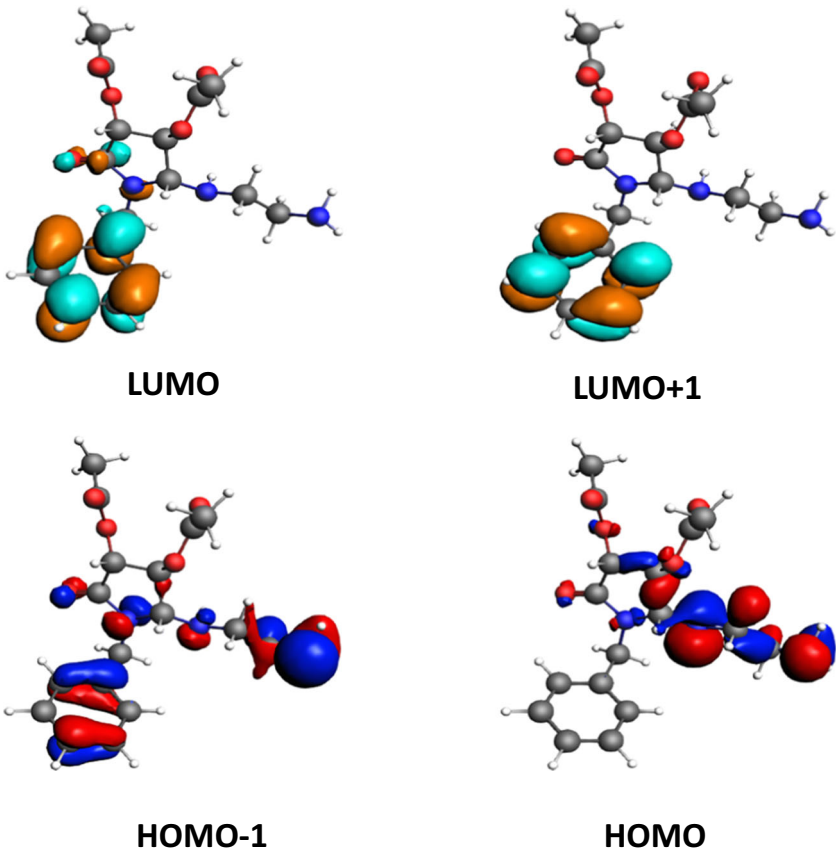

Fig. 8 Ground state charge density of FMOs of ligand (contour value = 0.035)

Table 2 The ground state HOMO energies (E_{HOMO}), LUMO energies (E_{LUMO}), energy gaps, EA,IP, μ, η, χ *S*, ω and IP ($-E_{HOMO}$) in eV of ligand.

Parameters	values
E_{HOMO}	−6.47
E_{HOMO-1}	−6.61
E_{LUMO}	−0.21
E_{LUMO+1}	−0.03
$\Delta E_{HOMO-LUMO}$	6.26
$\Delta E_{HOMO-1-LUMO+1}$	6.58
Hardness (η)	3.13
Potential (μ)	−3.34
Softness (*S*)	1.03
Electronegativity (χ)	3.34
Electrophilicity index (ω)	1.78
Ionization potential (IP)	6.47
Electron affinity (EA)	0.21

broadband arising from the boad ligand, indicating that the higher intramolecular energy transfer from the ligand to Tb^{3+} ion than recorded under excitation at 349 nm. It is noteworthy that the Tb^{3+} complexes exhibit very high intense green emission color, suggesting that organic ligands act as *antenna* chromophores.

Electronic Properties and Charge Analysis

The frontier molecular orbitals (FMO) i.e., HOMO and LUMOs have significant role to establish the charge transport and optoelectronic characteristics [29]. The spatial distribution of FMO within compounds plays a key role during effective charge injection. In the past, outcome of MO energies was investigated concerning recombination of excitons within OLED devices. These consequences disclose the fact that exciton recombination extremely sensitive to injection barriers, energy-level alignment along with charge mobilities. The LUMO levels have performed more critical role leading recombination dynamics compared with HOMO level. They designed efficient devices with suitable energy-level alignments [30]. Another approach to figure out the effect of electronic and optical characteristic is to examine the highest occupied molecular orbitals (HOMOs), and lowest unoccupied molecular orbitals (LUMOs) and energy gaps (E_{gap}) [31]. The FMOs, i.e., HOMOs, HOMOs-1, LUMOs, LUMOs+1 of ligand at B3LYP/TZ2P level are shown in Fig. 8**.** The spatial distribution of HOMO-1 is on (aminoethyl)amino and benzyl moiety, HOMO at (aminoethyl)amino and oxopyrrolidine, LUMO at carboxylic group and benzene ring, LUMO+1 at benzyl group. The intramolecular charge transfer (ICT) can be found from (aminoethyl)amino (HOMO-1) to benzyl moiety (LUMO and LUMO+1). The ICT was also detected from (aminoethyl)amino and oxopyrrolidine of HOMO to the benzyl group of LUMO and LUMO+1. Finally, the ICT was noticed from HOMO-1 → LUMO, HOMO-1 → LUMO+1, HOMO → LUMO, HOMO → LUMO+1 in the ligand. The electronic properties, nature of reaction or stability of molecules are interrelated to the spatial distribution of FMOs, especially HOMO. The charge density of HOMO on the (aminoethyl)amino moiety reveals the most credible sites in this ligand that can be definitely bombarded by nucleophiles.

The energies of FMOs, i.e., HOMO-1 (E_{HOMO-1}), HOMO (E_{HOMO}), LUMO (E_{LUMO}), LUMO+1 (E_{LUMO+1}), HOMO-LUMO energy gaps ($\Delta E_{HOMO-LUMO}$) and HOMO-1 – LUMO+1 energy gaps ($\Delta E_{HOMO-1-LUMO+1}$) are noteworthy parameters to discover the electronic properties of materials. The E_{HOMO-1}, E_{HOMO}, E_{LUMO}, E_{LUMO+1}, $\Delta E_{HOMO-LUMO}$ and $\Delta E_{HOMO-1-LUMO+1}$ of ligand at B3LYP/TZ2P level at ground state in eV are displayed in Table 2. The work functions (W) of Au and Al are 5.10 and 4.08 eV, respectively (http://www2.chemistry.msu.edu/faculty/harrison/cem483/work_functions.pdf, in). The hole/ electron injection energies (HIE/EIE) of ligand to Au and Al electrodes are probed. For Al, (EIE = $-E_{LUMO}$ − (W of Al) has been estimated as: (3.87 eV = −0.21− (−4.08)). In case of Au, (EIE = $-E_{LUMO}$ − (W of Au) has been estimated as: 4.89 eV = −0.21− (−5.10)).

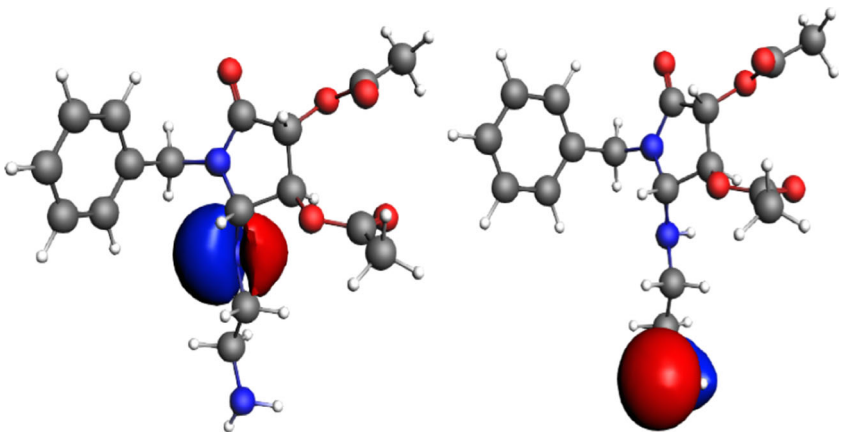

Fig. 9 NBO localized orbitals left (93) and right (94)

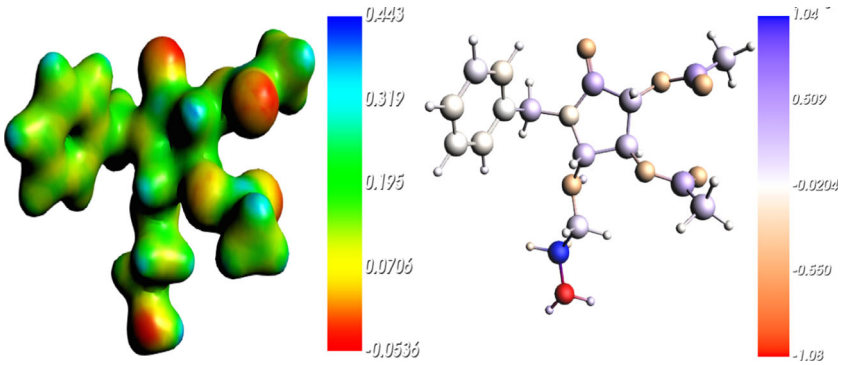

Fig. 10 Molecular electrostatic potential surfaces (top) and MDC-q charges (right) of ligand

The HIE was observed as 2.39 eV = −4.08 − (−6.47)) by considering Al electrode. In the case of Au, HIE was observed as (1.37 eV = −5.10 − (−6.47). One can see that for better electron/hole injection ability, Al/Au would be a more suitable electrode.

Global chemical reactivity descriptors (GCRD) are significant parameters to recognize the structure constancy and their reactivity. Here, we assessed numerous GCRD parameters e.g., electronegativity (χ), chemical potential (μ), chemical hardness (η), softness (S) and electrophilicity index (ω) of ligand, see Table 1 (computational particulars can be established in supporting information). The η of the compound is interrelated to aromaticity [32]. The μ express the electron's propensity to discharge within the electronic cloud. The η also represents the degree of the electronic cloud hindrance towards distortion, and ω signifies the stabilization energy of the coordination when electrons from the saturated peripheral atmosphere. The E_{gap} and reactivity descriptor parameters validate that the ligand would hold good reactivity to make complexes. Moreover, NBO analysis was carried out and presented in Fig. 9. One can see the NBO localized orbitals on N1 and N46 (numbering scheme can be found in supporting information), which illuminated that these sites would be favorable in the ligand to be attacked by the Eu and Tb to form complexes.

The Molecular Electrostatic Potential (MEP) maps are important to visualize the charged region of the compound. In Fig. 10, the MEP mapped for ligand has been illustrated in color visualizations. The red and blue color identifies negative and positive potential regions which would be promising for the electrophilic and nucleophilic attack, respectively. The robust -ive electrostatic potential is assigned within nitrogen and oxygen atoms, while the positive potential is determined on hydrogen atoms. The MDC-q charges of the ligand are illustrated in Fig. 10. The main negative charge can be found on the N46 (−1.070), N1 (−0.513), O10 (−0.546), O11 (−0.483), O13 (−0.530), O18 (−0.435), O20 (−0.479) atoms. The MDC-q charges revealed that N46 having maximum negative charge along with N-1 would be favorable sites for complex formation by Eu and Tb.

Conclusions

We have synthesized 1-benzyl-2-((2-Aminoethyl) amino)- 5-oxopyrrolidine-3,4-diyl diacetate, (boad) an oxopyrrolidine type ligand and designed to inoculate lanthanides [Eu^{3+} (**1**) and Tb^{3+} (**3**)] to get luminescent material. The target complexes showed good photoluminescence properties, which indicate that this type of compound can be used as luminescence sensitizers for the green (Tb^{3+}) and red (Eu^{3+}) emission. The results are evident that sensitizer efficiency can be improved by adding ligands like acac (**2**), which has also enhanced the luminescence quantum yields and lifetimes of Eu^{3+} ions. The intramolecular charge transfer was found from (aminoethyl)amino (HOMO-1) to benzyl moiety (LUMO and LUMO+1). The molecular electrostatic potential, NBO, MDC-q charges revealed that N46 having maximum negative charge along with N-1 would be favorable sites for complex formation by Eu and Tb. The exploration of optical properties having noteworthy multifunctional characteristics is revealing that the Tb^{3+}-complex would be proficient competitors for multifunctional semiconductor device applications, especially organic light-emitting diodes.

Acknowledgments M. Imran and M. A. Assiri extend their appreciation to the Deanship of Scientific Research at King Khalid University for funding through general research grant number GRP. 144/41.

References

1. Pelton M (2015) Light extraction from organic light-emitting diodes enhanced by spontaneously formed buckles. Nat Photon 9: 427–435. https://doi.org/10.1038/nphoton.2015.103
2. Bettencourt A, Viswanathan S, Rollet A (2007) Thiophene-Derivatized Pybox and its highly luminescent lanthanide ion complexes. J Am Chem Soc 129:15436–15437. https://doi.org/10.1021/ja076485
3. Li J, Li H, Yan P, Chen P, Hou G, Li G (2012) Synthesis, crystal structure, and luminescent properties of 2-(2,2,2-Trifluoroethyl)-1-indone lanthanide complexes. Inorg Chem 51:5050–5057. https://doi.org/10.1021/ic202473b
4. Mara D, Artizzu F, Laforce B, Vincze L, Hecke KV, Deun RV, Kaczmarek AM (2019) Novel tetrakis lanthanide β-diketonate

complexes: structural study, luminescence properties and temperature sensing. J. Lumin 213:343. https://doi.org/10.1016/j.jlumin.2019.05.035
5. Silva HRM, Faustino WM, Teotonio EES, Brito HF, Malta OL, Felinto MCFC (2019) Investigation on the formation of highly luminescent β-diketone-Ln(III)-EDTA water-soluble complexes. J. Lumin 207:182. https://doi.org/10.1016/j.jlumin.2018.10.021
6. Khan UL, Brito FH, Holsa J, Pirota RK, Muraca D, Felito MCFC, Teotonio EES, Malta OL (2014) Red-green emitting and Superparamagnetic Nanomarkers containing Fe_3O_4 functionalized with Calixarene and rare earth complexes. Inorg. Chem. 53:12902–12910. https://doi.org/10.1021/ic5018856
7. Faustino WM, Nunes LA, Terra IAA, Felinto MCFC, Brito HF, Malta OL (2013) Measurement and model calculation of the temperature dependence of ligand-to-metal energy transfer rates in lanthanide complexes. J. Lumin 137:269–273. https://doi.org/10.1016/j.jlumin.2013.01.008
8. Kovacs TA, Felinto MCFC, Paolini TB, Ali B, Nakamura LKO, Teotonio EES, Brito HF, Malta OL (2018) Synthesis and photoluminescence properties of [$Eu(dbm)_3$·PX] and [$Eu(acac)_3$·PX] complexes. J Luminescence 193:89–105. https://doi.org/10.1016/j.jlumin.2017.09.029
9. Lima GBV, Bueno JC, Silva AF, Neto ANC, Moura RTJ, Teotonio EES, Malta OL, Faustino WM (2020) Novel trivalent europium β-diketonate complexes with N-(pyridine-2-yl)amides and N-(pyrimidine-2-yl)amides as ancillary ligands: Photophysical properties and theoretical structural modeling. J. Lumin 219:116884. https://doi.org/10.1016/j.jlumin.2019.116884
10. Cortes MA, Cordier S, Naumov NG, Artznerc CMF, Molard Y (2014) Hexacyano octahedral metallic clusters as versatile building blocks in the design of extended polymeric framework and clustomesogens. J Mater Scince C 2:9813–9823. https://doi.org/10.1039/C4TC02098G
11. Lourenço AVS, Kodaira CA, Sanchez EMR, Felinto MCF, Goto H, Gidlund M, Malta OL, Brito HF (2013) Luminescent material based on the [Eu (TTA) sub (3)(Hsub (2) O) sub (2)] complex incorporated into modified silica particles for biological applications. J Inorg Biochem 123:11–17. https://doi.org/10.1016/j.jinorgbio.2013.02.006
12. Stefani HA, Ali B, Ferrera FP (2014) Ultrasound-assisted addition of alcohols to N-acyliminium ions mediated by In (OTf) $_3$ and synthesis of 1, 2, 3-triazoles. Tetrahedron Lett 55:3400–3405. https://doi.org/10.1016/j.tetlet.2014.03.104
13. Stefani HA, Ferrera FP, Ali B, Pimenta DC (2014) Synthesis of functionalized N-triazolyl maleimides. Tetrahedron Lett 55:4355–4358. https://doi.org/10.1016/j.tetlet.2014.05.095
14. Ali B, Schpector JZ, Ferrera FP, Shamim A, Pimenta DC, Stefani HA (2015) Lewis-acid catalyzed N-acyliminium ion cyclodimerization: synthesis of symmetrical 1, 4-dioxanes. Tetrahedron Lett 56:1153–1158. https://doi.org/10.1016/j.tetlet.2015.01.059
15. Ali B, Shamim A, Vasconcelos SNS, Stefani HA (2015) Synthesis and applications of 4-substituted 1-(4-iodophenyl) pyrrolidine-2, 5-diones. Tetrahedron Lett 56:4234–4241. https://doi.org/10.1016/j.tetlet.2015.05.066
16. Caracelli I, Schpector JZ, Stefani HA, Ali B, Tiekink ERT, (2015) Crystal structure of 1-benzyl-2-hydroxy-5-oxopyrrolidin-3-yl acetate. Acta crystallographic, section E, 71 (08):0582-0583. 10.1107/S205698 901 501 3 35 3
17. Irfan A, Chaudhry AR, Al-Sehemi AG, Assiri MA, Hussain A (2019) Charge carrier and optoelectronic properties of phenylimidazo[1,5-a]pyridine-containing small molecules at molecular and solid-state bulk scales. Comput Mater Sci 170:109179. https://doi.org/10.1016/j.commatsci.2019.109179
18. Irfan A (2019) Exploring the effect of oligocene elongation on photovoltaic, optoelectronic and charge transfer properties in tpa dyes tethered to the semiconductor surface. Results in Physics 13:102304. https://doi.org/10.1016/j.rinp.2019.102304
19. Irfan A, Kalam A, Chaudhry AR, Al-Sehemi AG, Muhammad S (2017) Electro-optical, nonlinear and charge transfer properties of naphthalene based compounds: a dual approach study. Optik-Intern J Light Elect Opt 132:101–110. https://doi.org/10.1016/j.ijleo.2016.12.023
20. Preat J, Jacquemin D, Perpète EA (2010) Design of new triphenylamine-sensitized solar cells: a theoretical approach. Environ Sci Technol 44:5666–5671. https://doi.org/10.1021/es100920j
21. Preat J, Michaux C, Jacquemin D, Perpète EA (2009) Enhanced efficiency of organic dye-sensitized solar cells: Triphenylamine derivatives. J Phys Chem C 113:16821–16833. https://doi.org/10.1021/jp904946a
22. Irfan A, Jin R, Al-Sehemi AG, Asiri AM (2013) Quantum chemical study of the donor-bridge-acceptor triphenylamine based sensitizers. Spectroch Acta A 110:60–66. https://doi.org/10.1016/j.saa.2013.02.045
23. Hasegawa Y (2014) Photofunctional lanthanoid complexes, coordination polymers, and nanocrystals for future photonic applications. Bull Chem Soc Jpn 87:1029–1057. https://doi.org/10.1246/bcsj.20140155
24. Binnemans K (2015) Interpretation of europium (III) spectra. Coord Chem Rev 295:1–45. https://doi.org/10.1016/j.ccr.2015.02.015
25. Neto ANC, Teotonio EES, de Sá GF, Brito HF, Legendziewicz J, Carlos LD, Felinto MCFC, Gawryszewska P, Moura Jr RT, Longo RL, Faustino WM, Malta OL, (2019) Handbook on the Physics and Chemistry of Rare Earths, 56:55–162. https://doi.org/10.1016/bs.hpcre.2019.08.001
26. Torresa JG, Jimenez PB, Calleja ET, Kennedy M, Ahmed H, Doran J, Tauste DG, Bautista L, Pirriera MD (2014) Highly efficient luminescent materials: influence of the matrix on the photophysical properties of Eu (III) complex/polymer hybrids. J Photochem Photobio A: Chem 283:8–16. https://doi.org/10.1016/j.jphotochem.2014.03.013
27. J. Kai (2009) Desenvolvimento de novos sistemas luminescentes à base dos polímeros PMMA e PHB dopados com complexos de terras raras. PhD Thesis Departamento de Química Fundamental, Instituto de Química - USP, São Paulo-SP.
28. Silva FA, Pereira H, Pereira DKS, Teotonio EES, Brito HF, Felinto MCFC, Espínola JG, Faustino WM (2013) Energy transfer processes in the Tb(III)-dibenzoylmethanate complexes with phosphine oxide ligands. J. Braz. Chem. Soc. 24:601–608. https://doi.org/10.5935/0103-5053.20130073
29. Wazzan N, Irfan A (2019) Exploring the optoelectronic and charge transport properties of pechmann dyes as efficient oled materials. Optik 197:163200
30. Yadav RAK, Dubey DK, Chen SZ, Liang TW, Jou JH (2020) Role of molecular orbital energy levels in oled performance. Sci Rep 10:9915
31. Jin R (2015) Theoretical study of the optical and charge transport properties of star-shaped molecules with 1,3,5-triazine-core derivatives as organic light-emitting and organic solar cells materials. Comptes Rendus Chimie 18:954–959
32. Geerlings P, Proft FD, Langenaeker W (2003) Conceptual density functional theory. Chem Rev 103:1793–1874. https://doi.org/10.1021/cr990029p